End-to-end sensor system modeling and validation for AR/VR/MR applications

Evan Kramer, Qing Chao, Michael Schaub, Song Chen, Wei Gao

Evan L. Kramer, Qing Chao, Michael Schaub, Song Chen, Wei Gao, "End-to-end sensor system modeling and validation for AR/VR/MR applications," Proc. SPIE 12415, Physics and Simulation of Optoelectronic Devices XXXI, 124150S (10 March 2023); doi: 10.1117/12.2668460

Event: SPIE OPTO, 2023, San Francisco, California, United States

End-to-end sensor system modeling and validation for AR/VR/MR applications

Evan L. Kramer [a], Qing Chao*[b], Michael Schaub[b], Song Chen[b], Wei Gao[b]
[a]MIT Dept. of Aeronautics and Astronautics, 77 Massachusetts Ave, Cambridge, MA, USA 02139
[b]Meta Reality Labs, 9845 Willows Rd NE, Redmond, WA, USA 98052-2540

ABSTRACT

Simultaneously prototyping several sensing architectures is costly and time consuming. Therefore, a modeling pipeline that is capable of both nanoscale electromagnetic wave and macroscale ray tracing simulations for the design, performance prediction, and validation of future AR/VR/MR sensing modalities is crucial. However, current end-to-end sensor modeling pipelines use several software packages with cumbersome interfaces between scene radiometry definition, macro optical component design, and photonics component design. In our paper, we demonstrate, implement and validate a sensor modeling pipeline with streamlined interfaces and modular component definition capabilities. The pipeline is composed of Ansys Speos for source radiometry and geometry definition, Zemax OpticStudio for camera lens system definition, and Lumerical FDTD for image sensor definition.

This end-to-end pipeline is used to model a camera system developed at Reality Labs and designed for AR/VR/MR applications. The first section of this paper describes the camera system modeled in the pipeline. Validation efforts for the pipeline involved comparing simulated images, obtained from inverse Monte Carlo ray propagation simulations, to experimentally collected images with the corresponding hardware. Specifically, the distortion and modulation transfer function (MTF) were determined for the simulated and experimentally collected images using ImaTest image quality software. The second section of this paper describes these validation efforts and the obtained results. The modularity of the modeling pipeline is highlighted throughout the paper for its applicability to various sensing architectures of interest to AR/VR/MR technologies.

Keywords: Validation, Image Simulation, Speos, Image Chain

1. INTRODUCTION

1.1 Ansys camera simulation pipeline

The Ansys camera simulation workflow enables modeling of all aspects in the imaging chain. As described by Fiete[1], the imaging chain models each step light takes from its source to the eventual post-processed image. At a high level, the steps are the radiometry characteristics of the source, macro-optical components such as lenses, photonic components such as sensors, and image processing[1]. To this end, Ansys Speos, Zemax OpticStudio, and Lumerical FDTD model these steps. The scene geometry and radiometry are modeled through CAD-based design and ray tracing in Ansys Speos. On the macro-optics scale, Zemax OpticStudio models how light is transferred through lens systems, including the effects of aberrations to the incident wavefront. On the photonics scale, active pixel sensor definition and efficiency is modeled in Lumerical FDTD. Simultaneous simulation of light behavior on both the macro and photonics level scales is prohibitively expensive in regard to computation time and space. Therefore, interfaces between Speos and FDTD enable ray tracing simulation results from Speos to be integrated with quantum efficiency results from FDTD simulations. Several methods describe interface techniques between ray tracing and photonics software packages[2,3,4], but these interfaces are cumbersome to incorporate into end-to-end workflows. The Ansys camera simulation workflow offers more streamlined interfaces using the Speos Lens System Importer (SLS) and Speos Sensor System (SSS) Importer. The SLS creates a reduced order model (ROM) of the full lens design specified in OpticStudio. The V2 version of the ROM incorporates a subset of higher order optical aberrations, including distortion, that is used to define the camera sensor in Ansys Speos. Additionally, the SLS exports a set of incidence angles to serve as inputs when defining plane wave sources in Lumerical FDTD. Alternatively, chief ray angle (CRA) data as a function of image height from OpticStudio can be used to manually specify the incidence angles. The SSS accepts irradiance and quantum efficiency maps as inputs and integrates the data to produce an electron map. Figure 1 shows the camera simulation workflow using the aforementioned software packages.

*qing.chao@meta.com

Physics and Simulation of Optoelectronic Devices XXXI, edited by Bernd Witzigmann,
Marek Osiński, Yasuhiko Arakawa, Proc. of SPIE Vol. 12415, 124150S
© 2023 SPIE · 0277-786X · doi: 10.1117/12.2668460

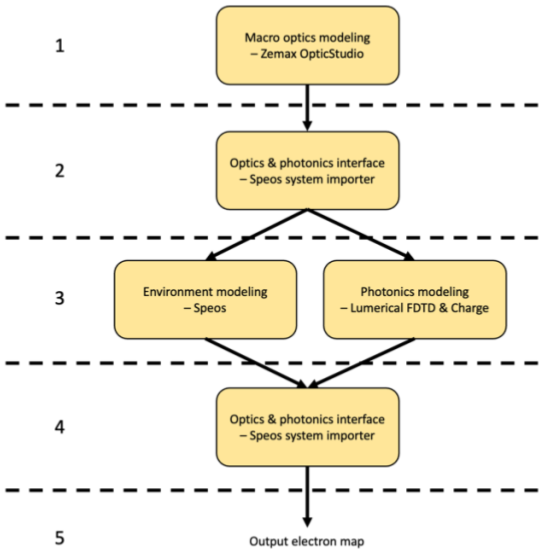

Figure 1. Camera simulation workflow with interfacing packages annotated[5].

The output of the macro optics portion of the pipeline, shown as the upper half of the workflow, is an irradiance map generated using a Monte Carlo algorithm. The output of the photonics portion of the pipeline, shown as the lower half of the workflow, is a map of quantum efficiencies generated using the Finite-Difference Time-Domain (FDTD) method. The final output of the workflow is an electron map that should closely match a real image captured using hardware analogous to the modeled components. Data from the irradiance map and quantum efficiency map are integrated according to equation 1 to produce the electron map.

$$N_c = t_{int} \int_{\lambda_{min}}^{\lambda_{max}} \frac{\lambda}{hc} EQE_{px}(\lambda) I(\lambda) A_{px} d\lambda \tag{1}$$

N_c is the number of electrons counted by the image sensor, t_{int} is the integration time, λ is the wavelength, h is Planck's constant, c is the speed of light, $EQE_{px}(\lambda)$ is the external quantum efficiency as a function of wavelength, $I(\lambda)$ is the irradiance as a function of wavelength, and A_{px} is the pixel area.

1.2 Sensor system

The camera lens was designed at Meta Reality Labs for VR/AR/MR applications. It has a focal length of 3mm and a circular FOV of 64°. The sensor was developed at Meta Reality Labs for application to AR/VR/MR sensor architectures. The sensor has a square focal plane with pixel pitch of 1.98um. The camera lens and sensor serve as the camera system considered in this work. The imaging system was designed such that the square dimensions of the sensor fit within the circular FOV at the focal plane of the camera lens. The motivation for underfilling the imaging system's FOV was the limited mass and volume resources available in the intended AR/VR/MR applications.

2. DATA COLLECTION SETUP

2.1 Experimental setup

To characterize the end-to-end performance of the camera lens and sensor imaging system discussed in section 1.2, a laboratory setup was constructed. The setup enabled control of the radiometric properties of the target and precise positioning of the lens and sensor components. A reflective 50.3in x 33.5in ImaTest ISO 12233:2017 Edge SFR target was rigidly mounted to a test stand. Two LED panels with color temperature control were oriented at 45° angles from the plane of the eSFR target. The color temperature of the LED panels was set to 5,100K. The eSFR target's optical scattering properties were considered to be Lambertian. All room lights were turned off during image acquisition and care was taken to minimize the presence of outside ambient light using blackout curtains. The camera lens and sensor were mounted on an aluminum breadboard and fixed to a stand attached to a translational railing. The sensor was mounted to a micrometer translation stage with ±10μm position precision. Figure 2 shows the hardware and laboratory setup.

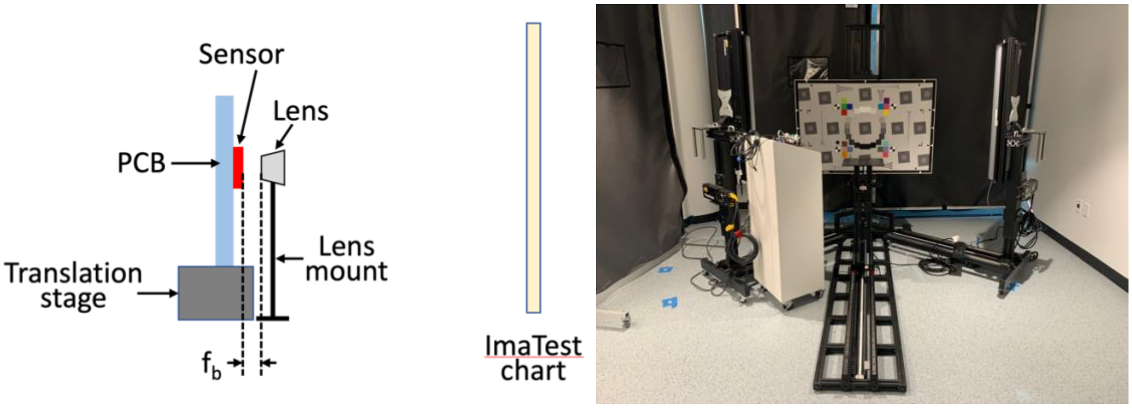

Figure 2. The camera lens and sensor mounted to an aluminum breadboard separated by the back focal length of the lens. The sensor board was mounted to a micrometer translation stage with ±10μm position precision (left). The ImaTest eSFR target mounted on a test stand along with two LED panels. The stand that the camera lens and sensor were attached to is shown in the center of the frame with the translational railing in the lower middle portion (right).

2.2 Simulation setup

The camera simulation pipeline was defined to match the experimental setup as closely as possible. In Speos, a digital, high resolution ImaTest eSFR target was used to define a display source. The display source dimensions were set to the dimensions of the experimental eSFR target and the radiant flux luminance was set to 500cd/m^2 with a 180° Lambertian intensity distribution. The white point of the display source was defined as the D50 standard daylight illuminant. The relative spectral power as a function of wavelength for D50 and D65, another common standard daylight illuminant is shown in figure 3.

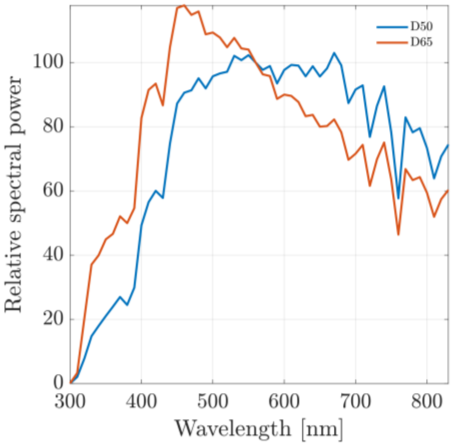

Figure 3. Relative spectral power as a function of wavelength for D50 and D65 standard daylight illuminants.

A camera sensor was defined with optical and sensor level properties corresponding to experimental and modeling-based data for the camera lens and sensor. For the camera lens optics, a focal length of 1.061mm and F-number of 2 was specified with a V2 distortion file and optical coating transmission spectrum. For the sensor, a focal plane of 640px x 640px was defined over a square detector with side length 2.534mm. Additionally, the sensor was defined as a monochrome sensor with a spectral sensitivity corresponding to experimentally collected data. The camera sensor was defined to sample 8 wavelengths from 400nm to 1,100nm in steps of 100nm. Figure 4 shows the experimentally determined camera coating transmission spectrum and the sensor spectral sensitivity.

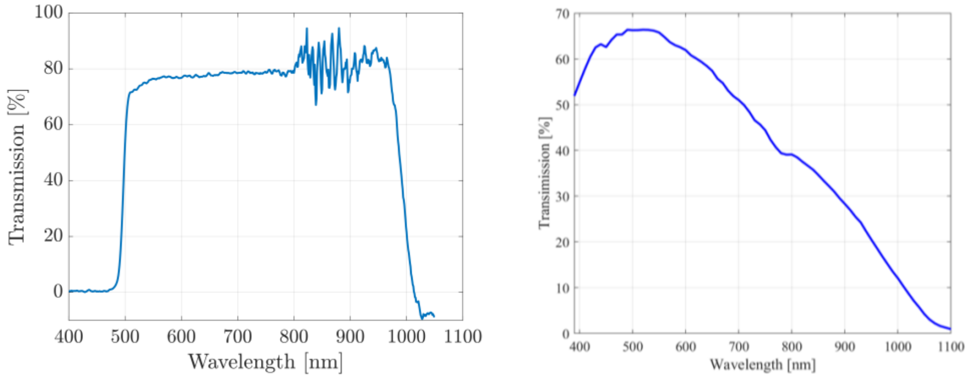

Figure 4. Experimentally determined camera coating transmission spectrum (left) and experimentally determined sensor spectral sensitivity (right) used to define the camera sensor in Speos.

The focal point of the camera sensor was positioned at the origin of an inertial frame. Relative to the inertial frame origin, the display source was positioned in the center of the camera sensor's FOV a distance of 60cm away and oriented normal to the camera's principal axis. Figure 5 shows the simulation setup in Speos with a grid projection of the camera sensor FOV.

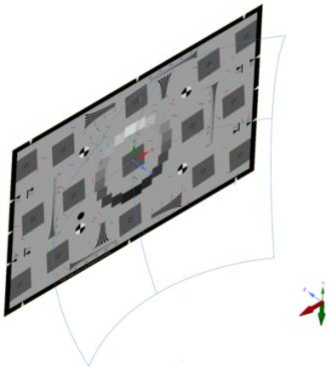

Figure 5. Simulation setup in Speos. The camera sensor is defined at the origin of the inertial frame with its principal axis oriented normal to the target plane. The blue grid shows the projection of the camera sensor FOV at a radial distance of 60cm.

A simplified model of a representative pixel for the sensor used during experimental data collection was created in Lumerical according to the dimensions shown in figure 2 for FDTD simulations. An idealized photon to electron weighting factor was specified such that any photon incident on the photoactive portion of the pixel was converted to an electron. A plane wave source was defined with a maximum incidence angle equal to the maximum CRA from the camera lens and a spectral range equal to the 400nm to 1,100nm range defined for the camera sensor in Speos. Figure 6 shows a 2-dimensional profile of the modeled pixel quadrant.

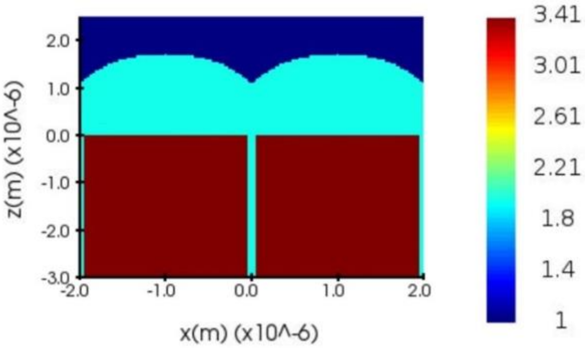

Figure 6. Cross section of simplified model of pixel quadrant in Lumerical.

It was mentioned in section 1.1 that the output of the FDTD simulations was a map of quantum efficiencies. Three different quantum efficiencies are output by FDTD. The optical efficiency (OE) is the ratio of absorbed photons to incident photons. The internal quantum efficiency (IQE) is the ratio of collected charge to generated charge. Finally, the external quantum efficiency (EQE), is the product of the OE and IQE. The EQE map is the data set used to compute the electron map. All three efficiencies are functions of wavelength, angle of incidence, θ, and azimuthal angle, $\emptyset$. Figure 7 shows the OE, IQE, and EQE for a coarse FDTD simulation of the simplified sensor model.

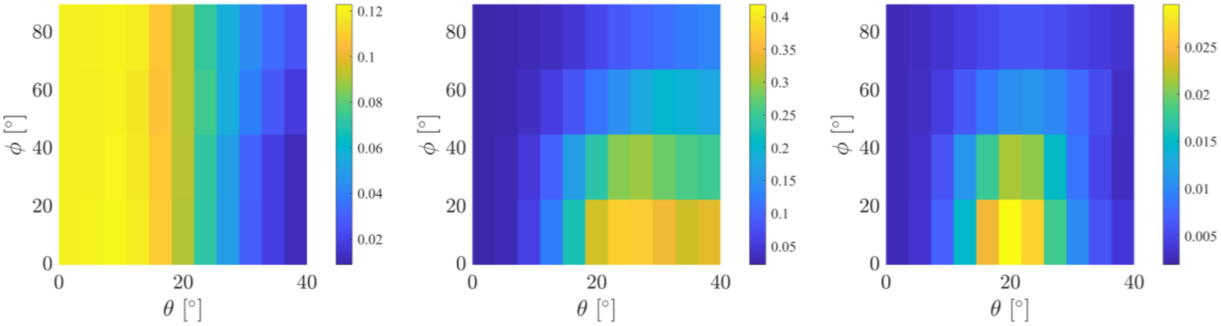

Figure 7. OE (left), IQE (middle), and EQE (right) for a coarse FDTD simulation of the simplified sensor model.

3. SIMULATION VALIDATION

A variety of image quality metrics can be used when comparing different images. This work considered two metrics, geometric distortion and MTF, during validation of the camera simulation pipeline. Geometric distortion was considered due to the significant amount present in many wide-angle lenses including the camera lens used in this work. MTF was considered because it is a popular system-level image quality metric and can reliably be used to compare different imaging systems. The ImaTest software suite was used to extract and record data on these metrics. Identical processing settings were used for the experimental and simulated images. The following subsections describe the validation of the camera simulation pipeline using these metrics.

3.1 Geometric distortion

Lens geometric distortion (LGD) is primarily due to lens aberrations from the macro-optics components of the camera system. Therefore, to validate the distortion modeling of the macro-optics components in Speos, geometric distortion percentage as a function of sensor position was computed for simulated images and compared with camera lens geometric distortion data from Zemax OpticStudio. Geometric distortion percentage is computed according to equation 2.

$$LGD = \frac{(r_d - r_u)}{r_u} \times 100\% \qquad (2)$$

The r_d and r_u terms correspond to the radial positions of a particular feature in the distorted and undistorted images respectively. The positions are normalized to the center-to-corner distance in the image plane. ImaTest provides test charts intended for use in determining the distortion parameters of a camera system. These test charts contain features, such as line intersections or points, that occur in regular patterns. A high resolution ImaTest checkerboard target was uploaded to the display source in Speos and resized such that its dimensions filled the camera's field of regard. A simulated image of the checkerboard target was recorded and the ImaTest chart analyzer was used to fit several distortion models to the simulated image. The distortion models include 3rd and 5th order polynomials and a tangent model for barrel distortion respectively. Figure 8 below shows a plot of the LGD as a function of the normalized distorted image center to corner distance for the distortion models and OpticStudio data for the camera lens.

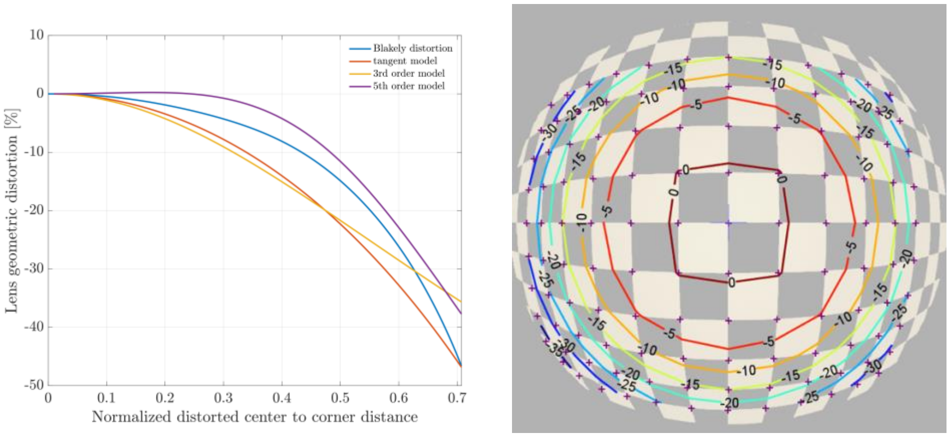

Figure 8. LGD as a function of normalized distorted image center to corner distance. The x-axis limit corresponds to the top and bottom edges of the sensor corresponding to the maximum extent of the camera lens FOV in the image plane (left). LGD contour map for simulated image of checkerboard distortion target (right).

The x-axis limit corresponds to the top and bottom edges of the sensor corresponding to the maximum extent of the camera lens FOV in the image plane. While none of the plotted distortion models match the camera lens distortion curve over all radial distances, the 5th order model shows a similar general trend and the tangent model, which is often used to model distortion in fisheye lenses, matches the camera lens LGD at the top and bottom edges of the sensor. Given the simplicity of these distortion models, deviation from the true camera lens distortion was expected. For the purposes of an initial validation of the end-to-end sensor system model, the results show that the camera lens distortion is modeled by the V2 Speos distortion file.

3.2 Spatial frequency content

Although it is not a standard image quality metric, another image comparison tool is the transfer of spatial frequency content through the optical system. Lens aberrations, sensor sampling, and other factors contribute to limiting the transfer of features with certain spatial frequencies in object space. Several targets were created in Matlab with periodic intensity distributions of various frequencies. Figure 9 shows the initial target image and the simulated image.

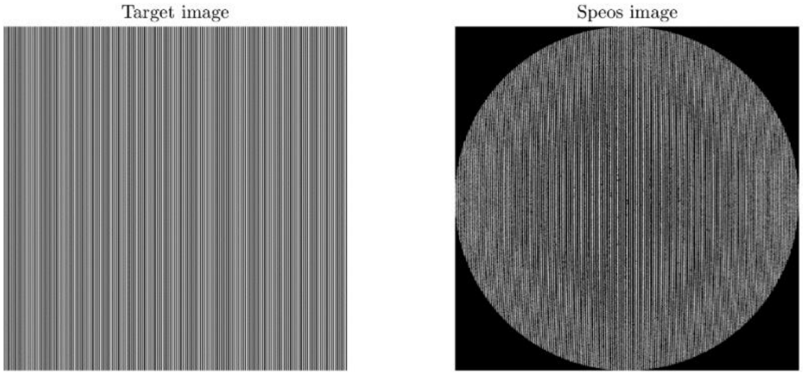

Figure 9. The initial sinusoidal target image with a predefined spatial frequency is shown on the left with the corresponding simulated image of the target created using a display source in Speos.

These targets were uploaded to the display source in Speos and sized such that the instantaneous field of view, IFOV, of a single pixel in the camera sensor subtended the area of a single pixel in the target image. Simulated images were recorded and loaded into Matlab. The 1-dimensional discrete Fourier Transform was taken of a 1-dimensional array of pixels sampled horizontally from the center 40% of the image. Due to the significant amount of barrel distortion in the camera lens as shown in section 3.1, a shift in the Fourier spectra of the simulated images was anticipated. The average amount of distortion was computed based on the fraction of the image used in the 1-D array. For 40% image usage, the average distortion is −6.1%. A spatial frequency scaling factor corresponding to the average distortion was applied to each simulated image Fourier spectrum. Figure 10 shows the distortion shifted, normalized Fourier Transform of the simulated image 1-D pixel array for three different targets with unique spatial frequencies along with the normalized Fourier Transform of the three initial images.

As expected, the Fourier spectra of the three target images, plotted as black dashed lines, have singular spikes at the respective periodic intensity distribution frequencies. The Fourier spectra of the simulated image 1-D pixel arrays show wider and noisier spatial frequency spectra due to the modeled optical lens aberrations and random noise from Monte Carlo propagation. The peaks of the simulated image and target image spectra overlap, indicating that the spatial frequencies of features in the target images were transferred through the optical system without manipulation in the spatial frequency domain. This result provided additional confidence in the camera lens optical distortion model used to define the camera sensor in Speos.

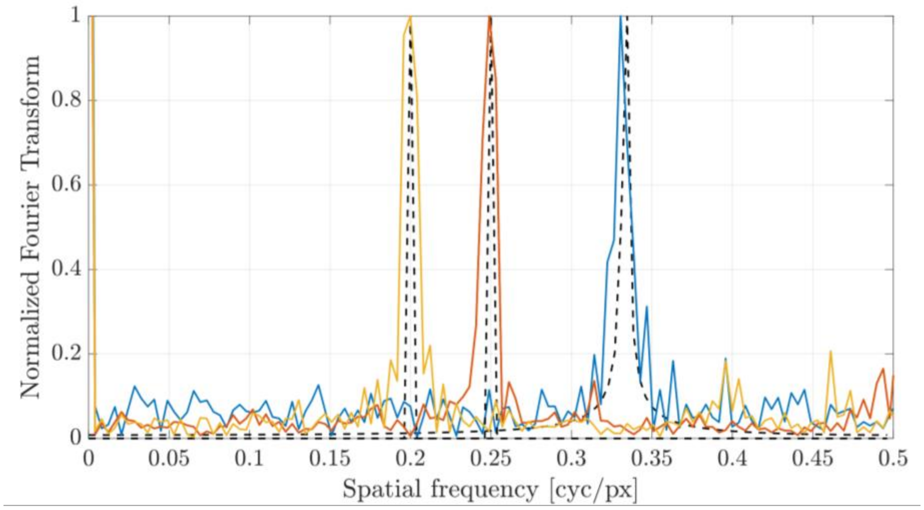

Figure 10. Normalized Fourier spectra of 1-dimensional pixel array in simulated images. Blue, red, and yellow curves correspond to 1/3, 1/4, and 1/5 cyc/px target image spatial frequencies. Black dashed curves show the normalized Fourier spectra of the target image spatial frequencies.

3.3 MTF

One of the most fundamental image quality metrics is sharpness. Sharpness describes the amount of detail an image can convey and is mathematically expressed as the modulation transfer function (MTF). The MTF considers the modulation, or contrast of an image according to equation 3.

$$MTF = \frac{(I_{max} - I_{min})(O_{max} + O_{min})}{(O_{max} - O_{min})(I_{max} + I_{min})} \tag{3}$$

The maximum and minimum image and object irradiances are denoted as $I_{max}, I_{min}, O_{max},$ and O_{min} respectively. There are several ways in which the MTF of an imaging system can be measured. The approach taken in this work is the slant edge method[6]. The ImaTest analyzer tool computes the MTF for any subset of the slanted edges in the eSFR target and applies several averaging and smoothing techniques for improved accuracy[7]. The ImaTest analyzer tool was used to compute MTFs for simulation pipeline validation purposes.

Whereas the previous results presented on geometric distortion and spatial frequency content considered only optical aberrations, the MTF results presented in this section take into account image quality degradation contributions from both macro-optical components and photonics components. As discussed in section 1.1, an electron map is produced by the camera simulation pipeline. Figure 11 shows the electron map and experimental image used for MTF comparisons in this work.

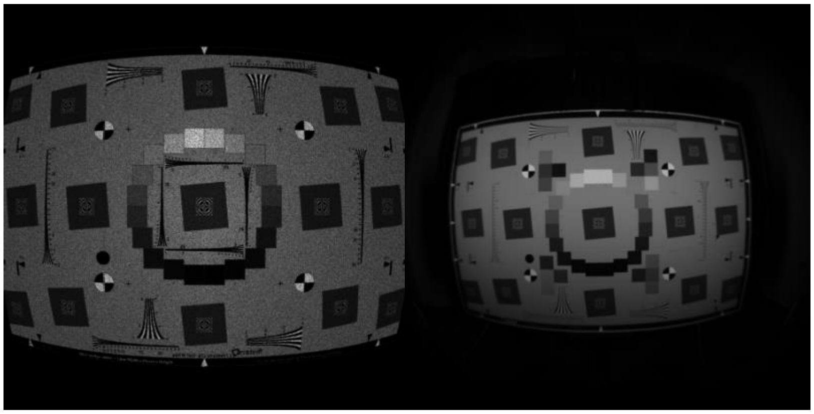

Figure 11. Simulated electron map of eSFR target (left) and experimental image of eSFR target (right).

The eSFR target appears to occupy a larger area of the camera's FOV compared to the eSFR target in the experimental image. This is due to a cropping of the sensor that involved reducing the number of pixels defined in the Speos camera sensor such that the square sensor was completely inscribed by the camera lens image plane. This cropping was necessary to enable electron map generation due to current limitations for processing images with underfilled FOVs in the Speos simulation pipeline. Care was taken to ensure the pixel pitch was kept constant despite the cropping of the sensor.

The MTFs of different camera systems can be directly compared when the maximum spatial frequency resolvable by the optics and the maximum sampling frequency set by the sensor are equivalent. The Q factor is the ratio of these two frequencies and is defined as shown in equation 4.

$$Q = \frac{2\xi_N}{\xi_C} \tag{4}$$

The cutoff frequency for a circular aperture imaging system is $\xi_C = {}^{1}\!/_{(\lambda f/D)}$ where λ is the wavelength, f is the focal length, and D is the aperture diameter. The detector sampling frequency is $\xi_N = {}^{1}\!/_{p}$ where p is the detector pixel pitch. As long as ξ_C and ξ_N remain constant between camera systems, a direct comparison can be made.

Before presenting results comparing the experimental MTF to simulated image MTF, uncertainty bounds for both curves were determined by considering the respective sources of uncertainty. The inverse Monte Carlo ray propagation introduces random noise into the simulated images resulting in variations in MTF primarily towards high spatial frequencies. To quantify the amount of MTF variation as a function of spatial frequency, 20 simulated images were recorded. ImaTest image analyzer was used to compute MTFs for each of the 20 simulated images for two regions of interest (ROI). ROI 1 corresponds to the top horizontal slanted edge of the central square in the eSFR target while ROI 3 corresponds to the right vertical slanted edge. In addition to computing the MTFs for each of the simulated images, the MTF for the average signal was computed using the average signal feature in ImaTest. Figure 12 shows plots of the individual and average signal MTF curves for ROI 1 and ROI 3.

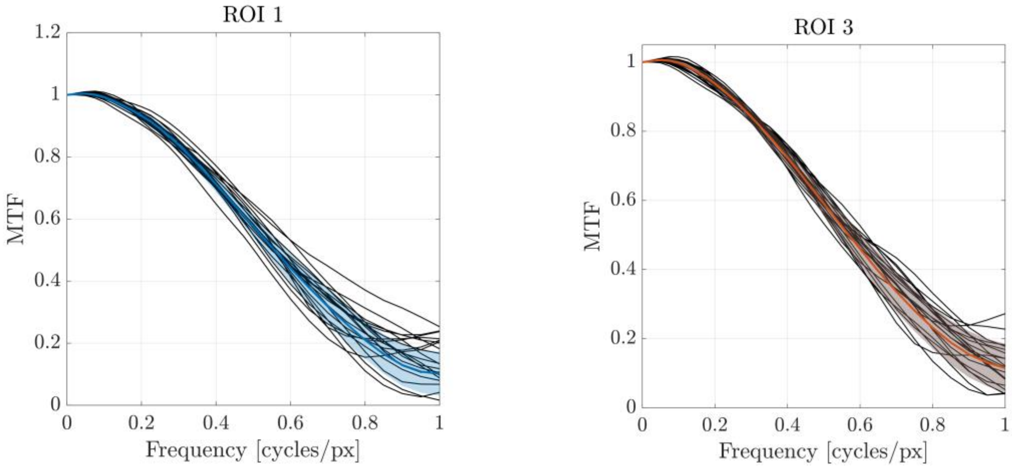

Figure 12. Individual and average signal MTF curves for ROI 1 and ROI 3. Individual image curves are plotted in black, average signal curves are plotted in blue and red, and the ±1σ standard deviation is shown in faded blue and red.

As expected, the MTF curves start at 1 and decrease towards 0 as the spatial frequency increases. The variation between the individual image MTFs represented by the black curves increases as the spatial frequency increases. This is also expected since random noise contributed by the Monte Carlo algorithm does not contribute low spatial frequency-structured features to the simulated images. Qualitatively, the average signal MTF is observed to represent the overall trend of the individual MTF curves with an increasing standard deviation. To discern the variation of MTF as a function of spatial frequency more clearly, the ±1σ standard deviation in the individual MTF curves was computed as a function of spatial frequency for both ROIs and plotted in figure 13.

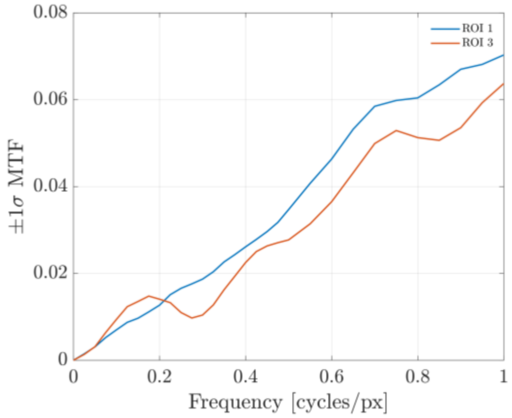

Figure 13. ±1σ standard deviation of the individual MTF curves as a function of spatial frequency for ROI 1 and ROI 3.

The primary contributor to MTF uncertainty in the experimental images is attributed to uncertainty in the position of the sensor relative to the camera lens. Experimental images were collected for a sequence of sensor positions to find best focus. As discussed in section 2.1, the micrometer used to increment the position of the sensor had a precision of ±10μm. The MTF varies significantly for imaging systems with focus variability. To quantify the MTF degradation due to position error of the sensor plane, a through focus MTF plot was created for the camera lens at several spatial frequencies and the resulting MTF degradation was plotted as a function of spatial frequency for two position error shifts in figure 14.

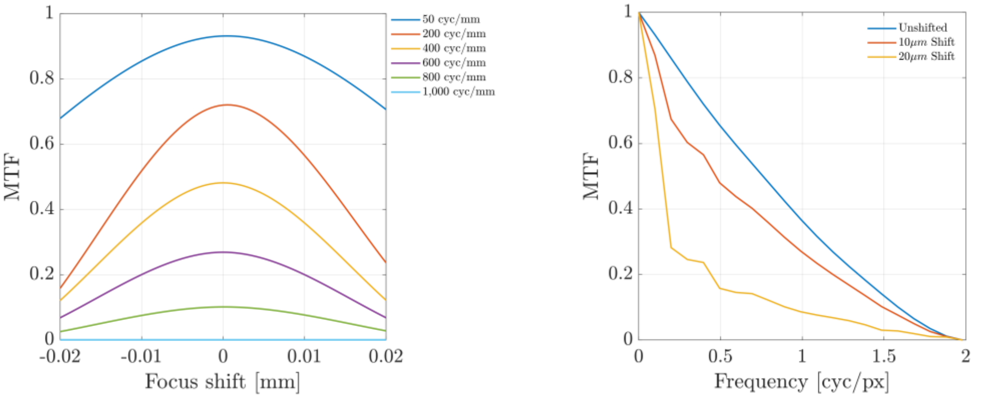

Figure 14. Through focus MTF plot for several spatial frequencies (left) and the degradation in MTF as a function of spatial frequency for unshifted, 10μm, and 20μm shifts (right).

Having quantified the primary sources of uncertainty present in the experimental and simulated MTF curves, an informed comparison between the curves could be made. The MTF curves for both the simulated electron map and irradiance maps were plotted along with the ±1σ uncertainty bounds. The MTF curve corresponding to the sharpest experimental image for all spatial frequencies was selected and used for comparison to the simulated image MTF curve. Due to the ±10μm precision of the sensor, an uncertainty bound corresponding to the degradation in MTF caused by a 10μm shift was plotted. An additional comparison to the simulated and experimental MTF curves was made with the diffraction limited MTF curve for the camera lens. The geometric diffraction limited MTF curve from OpticStudio, which is a Fourier transform of the lens geometric spot data and does not consider diffraction effects, served as the geometric MTF curve in figure 15. All curves are plotted in figure 15 for comparison.

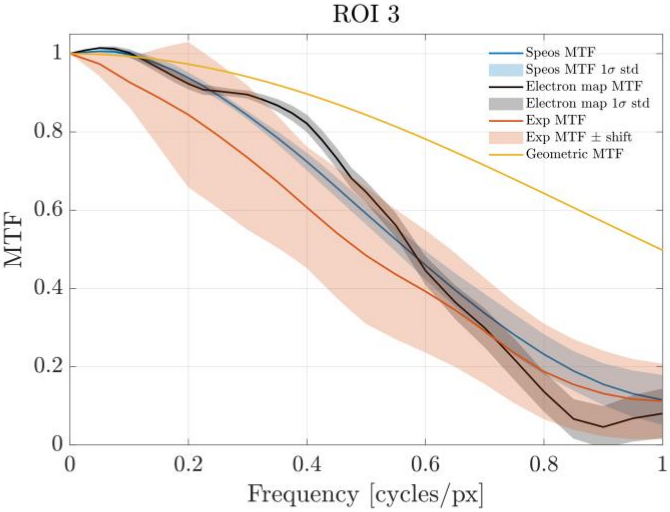

Figure 15. MTF curves plotted for comparison. All curves computed for eSFR target ROI 3.

As expected, the geometric diffraction limited MTF curve outperforms the MTF curves for the experimental and simulated images. The blue MTF curve for the irradiance map trends with the black MTF curve for the electron map. At spatial frequencies greater than 0.6cycles/px, the electron map MTF is outperformed by the irradiance map MTF. This sharpness degradation is likely due to incorporation of sensor efficiencies in the electron map generation that are not modeled in the irradiance map MTF. The electron map MTF outperforms the irradiance map MTF between spatial frequencies of 0.22cycles/px and 0.6cycles/px. This deviation is likely not due to any physical behaviors being modeled in electron map generation, but rather a result of computing the MTF of two different images created using Monte Carlo techniques. Both the electron map and irradiance map MTFs outperform the experimental MTF for spatial frequencies up to 0.7cycles/px. Both simulated image MTF curves are contained within the experimental MTF uncertainty bounds for almost all spatial frequencies. At the time of writing, a preliminary study being conducted by Ansys indicated that the camera sensor reduced order model approximates geometric aberration impacts on image sharpness from coma and astigmatism as a Gaussian and does not fully support chromatic aberration modeling. The approximations and assumptions present in the camera sensor reduced order model likely contribute to the discrepancy observed between the Speos-produced MTFs and the experimental and geometric MTFs. Overall, the MTF trends indicate that the system-level camera performance being simulated by the camera simulation pipeline is in agreement with experimentally collected data. While additional work is needed to reduce the magnitude of the uncertainty bounds present in the simulated and experimental data sets, these results serve as an initial validation of the camera simulation pipeline.

4. CONCLUSION AND NEXT STEPS

In this paper, an end-to-end camera simulation pipeline is described. The pipeline offers improved modularity and streamlined interfaces between radiometric, macro optics, and photonics modeling software packages compared to other end-to-end camera simulation pipelines. An image quality test setup was defined in the simulation pipeline for a camera lens and sensor system specifically designed for AR/VR/MR applications. High level descriptions of the modeled components were given, specifically for the camera lens and the image sensor. The simulation pipeline was used to produce simulated irradiance and electron maps of test targets. An initial validation of the simulation pipeline was presented by comparing image quality metrics computed for simulated images with results for images collected using hardware in an analogous laboratory environment using ImaTest image quality software. Lens geometric distortion was computed for simulated images and fit to several distortion models. The simplified, fitted distortion models demonstrated that the distortion of the camera lens was being modeled in the camera sensor definition and that a more complex model would be needed to accurately fit the lens distortion for all sensor radial positions. System MTF was computed for the simulated irradiance and electron maps and uncertainty bounds were determined. Similarly, an uncertainty bound was determined for error in sensor positioning and applied to the MTF curve for an experimental image. Comparisons were made between simulated, experimental, and theoretical best performance MTF curves. The presented MTF results serve as an initial validation of the end-to-end Ansys Speos camera simulation pipeline. Additional work is needed to further validate the simulation pipeline. The following lists next steps for this work.

1. Run FDTD simulation for sensor with increased spatial and spectral sampling to reduce the amount of interpolation of quantum efficiencies between spatial and spectral samples.
2. Incorporate microlens shift in FDTD model and compare simulation and experimental relative illumination results. Relative illumination comparisons will serve as an additional camera simulation validation metric.
3. Import a full CAD model of the camera lens into Speos and define an irradiance sensor at the corresponding image plane to quantify differences in full system MTF performance compared to Speos camera sensor ROM.

REFERENCES

[1] Robert D. Fiete and Bradley D. Paul. Modeling the optical transfer function in the imaging chain. Optical Engineering, 53(8):083103, 2014.

[2] Axel Crocherie, James Pond, Federico Duque Gomez, Kevin Channon, and Frederic Fantoni, "Micro to macro scale simulation coupling for stray light analysis," Opt. Express 29, 37639-37652 (2021).

[3] C. Leiner, S. Schweitzer, F. -P. Wenzl, P. Hartmann, U. Hohenester and C. Sommer, "A Simulation Procedure Interfacing Ray-Tracing and Finite-Difference Time-Domain Methods for a Combined Simulation of Diffractive and Refractive Optical Elements," in Journal of Lightwave Technology, vol. 32, no. 6, pp. 1054-1062, March 15, 2014, doi: 10.1109/JLT.2013.2297411.

[4] Guillaume Chataignier, Benoit Vandame, and Jérôme Vaillant, "Joint electromagnetic and ray-tracing simulations for quad-pixel sensor and computational imaging," Opt. Express 27, 30486-30501 (2019).

[5] CMOS Sensor Camera – Image Quality Analysis in a 3D Scene, Ansys, https://optics.ansys.com/hc/en-us/articles/8195614998547-CMOS-Sensor-Camera-Image-Quality-Analysis-in-a-3D-Scene, 2022.

[6] Peter D Burns et al. Slanted-edge mtf for digital camera and scanner analysis. In Is and Ts Pics Conference, pages 135–138. Society for Imaging Science & Technology, 2000.

[7] Norman Koren. The Imatest program: comparing cameras with different amounts of sharpening. In Nitin Sampat, Jeffrey M. DiCarlo, and Russel A. Martin, editors, Digital Photography II, volume 6069, page 60690L. International Society for Optics and Photonics, SPIE, 2006.

[8] Andy Cochrane, Kevin Schulz, Rick Kendrick, and Ray Bell, "Q Selection for an electro-optical earth imaging system: theoretical and experimental results," Opt. Express 21, 22124-22138 (2013).